Astron. Astrophys. 356, 41–49 (2000)

ASTRONOMY AND ASTROPHYSICS

Arp 102B: variability patterns of the Hα line profile as evidence for gas rotation in the broad-line region

S.G. Sergeev, V.I. Pronik, and E.A. Sergeeva

Crimean Astrophysical Observatory, P/O Nauchny, 98409 Crimea, Ukraine
Isaac Newton Institute of Chile, Crimean Branch

Received 9 August 1999 / Accepted 3 January 2000

Abstract. We present results of an optical spectral monitoring campaign of the Seyfert 1 galaxy Arp 102B for a period of about 4 years between 1992 July and 1996 October carried out with a CCD spectrograph at the 2.6-m Shajn Telescope of the Crimean Astrophysical Observatory. Our data set consists of 20 Hα and 1 Hβ region spectra. During the monitoring period, the Hα line and continuum fluxes have shown the root mean square (rms) variations as small as 2.7% and 5.7%, respectively. The Hα line lag greater than 66 days is ruled out at 99% confidence level. Strong rms variations at different bins of the Hα profile (5–10%), while its total flux is changed only a little can be explained by the rotational redistribution of matter emitted the broad lines. We consider two possibilities: a continuous disk with inhomogeneities in its surface brightness and a system of clouds rotating predominantly in the same plane. Different sections of the line profile generally show very poor correlation between themselves as well as with the continuum flux, while the correlation between the line integrated flux and continuum flux is much better. The line component that respond to the continuum changes is probably more prominent in the red central part of the line profile, where the correlation with the continuum fluxes is somewhat better. Some indications of the rotation are also seen from the evolution of the residuals between each normalized profile and the mean normalized profile. Typical timescale of rotation (~ 1000 days) suggests a very large mass of the central body of about $3.5 \times 10^8\,\mathrm{M}_\odot$.

Key words: galaxies: active – galaxies: individual: Arp 102B – galaxies: nuclei – galaxies: quasars: emission lines – galaxies: Seyfert

1. Introduction

The structure and kinematic of the broad-line region (BLR) in active galactic nuclei (AGNs) is still poorly known. Even the most extensive monitoring campaigns (e.g. Wanders & Peterson 1996; Peterson et al. 1999; Maoz et al. 1991; Kaspi et al. 1996) have not yielded conclusive results by using the reverberation mapping approach (Blandford & McKee 1982; Peterson 1994). The broad emission lines in AGNs show a variety of profile shapes that can strongly vary in time. A relatively small group of objects have double-peaked components that are widely spaced in velocity, e.g.: 3C 390.3, Arp 102B, 3C 332, Pictor A. A double-peaked profile can be reproduced with the relativistic Keplerian disk (Chen et al. 1989), the outflow streams (Zheng et al. 1991), the Keplerian orbiting clouds irradiated by the anisotropic continuum source (Goad & Wanders 1996), or the double black hole (Gaskell 1988). A variety of the broad-line profiles can also be reproduced with the hydromagnetic wind model (Emmering et al. 1992). Surely, each model has a different validity in theoretical aspects as well as in observational aspects and the task of observers is to eliminate from consideration those models that have failed basic observational tests. The double black hole model should probably be rejected because hump wavelengths should drift with time. Eracleous et al. (1997) have found no such long-term systematic changes in radial velocity in Arp 102B, 3C 390.3, and 3C 332 during two decades of observations. Their result suggests a lower limit of the total binary mass of $10^{10}\,\mathrm{M}_\odot$ that difficult to reconcile with observations and theory. Moreover, the line profile produced by BLR in a double system is not a sum of profiles of two single systems. A drawback of the model of randomly orbiting clouds proposed by Goad & Wanders (1996) is that the clouds should have large sizes as well as internal velocity dispersion to provide an appropriate covering factor and smooth line profiles. Such clouds may dissipate or collide in a short time. The Keplerian disk model (without assumption of hot spots, see below) yields simultaneous variations and constant flux ratio of the red and blue humps, inconsistent with observations. The model of outflow steams is not supported by reverberation mapping studies, since it is not found that the red wing lags behind the blue wing. Patterns of long-term variations should eventually enable to distinguish these models.

3C 390.3 and Arp 102B were the first AGNs, the BLR of which was proposed to be the relativistic accretion disk because of its extremely broad double-peaked Balmer line profiles (Oke 1987; Perez et al. 1988; Chen et al. 1989; Chen & Halpern 1989). The principal features of such a profile are: the red peak is lower and more extended, while the blue peak is stronger and steeper. The profile asymmetry is due to the relativistic and gravitational effects. However, the red bump can be

Send offprint requests to: S.G. Sergeev (sergeev@crao.crimea.ua)

brighter than the blue bump if a disk is not circular, but elliptical (Eracleous et al. 1995). At the present time, a total of 12 cases are known for which the Balmer line profiles are reasonably well fitted by the accretion disk model assuming a power-law dependence of the surface brightness on distance (Eracleous & Halpern 1994). The line emission of the accretion disk at each radius was computed by Collin-Souffrin & Dumont (1990) who have found that the broad low-ionization lines in Seyfert galaxies and low-luminosity quasars can be almost entirely attributed to the disk. The ionizing continuum source was assumed to be above the disk.

Newman et al. (1997) have monitored the behavior of the optical emission-line spectrum of Arp 102B for more than 13 years in order to test the accretion disk and other models. They found an interval during which the variation in the ratio of the fluxes of the two peaks appeared to be sinusoidal, with a period of 2.16 years and amplitude of about 16%. The sinusoidal variation has been attributed to the moving excess emission produced by a "hot spot" in the accretion disk. They have also attempted to detect this emission and to watch its evolution. However, their results seem to be not reliable because of the internal and external disk radii were assumed to be variable. Under such assumption there are too many possibilities to detect any excess emission in the line profile.

Our spectral monitoring program on Arp 102B was primarily undertaken in order to look for the changes in the profile shape of the broad Hα line. The Hα line and continuum light curves are present in Sect. 3, the cross-correlation results are given in Sect. 4, and the variability patterns of the profile shape are considered in Sect. 6.

2. Observations and data processing

Our spectral monitoring of Arp 102B has been carried out at the Crimean Astrophysical Observatory on the 2.6 m Shajn Telescope since 1992. The observations and instrumentation as well as the spectral data processing are described in detail in the papers of Malkov et al. (1997) and Sergeev et al. (1999a). All the spectra were obtained with the position angle of the entrance slit of 90° (aligned on right ascension). The entrance slit width was set to 3″.0, excluding the first two spectra obtained with the slit width of 2″.0. We estimated the spectral resolution of our spectra to be 7–8 Å except for a one case where it was equal to more than 10 Å. The "extraction window" was set to 11″. Our data set consists of 20 flux-calibrated spectra in the Hα spectral region and only a single spectrum in the Hβ region. The spectra were obtained with a single exposure within a night. The exposure time was of about 50–100 minutes. We have estimated the signal-to-noise ratio (S/N) per pixel at the continuum level to be in range 25–55 with the mean value of 36.

3. Calibration and measurements of spectra

We have followed the commonly used calibration method based on the assumption that the narrow emission lines are constant in flux. The most appropriate narrow emission line in the Hα region is [O I] λ6300. However, we have estimated that the calibration uncertainties should be, on average, as much as 4% and decided, therefore, to use the narrow Hα and [N II] lines that are remarkably brighter and provide a better precision of calibration. Since these lines are not single but superposed on the broad Hα emission-line profile we have implemented the calibration method based on the subtraction of a reference spectrum (van Groningen & Wanders 1992; Sergeev 1992). A scale factor for each spectrum with respect to the reference spectrum was found by optimizing the smoothness of the residuals in the wavelength window of 6680–6775 Å (all the wavelength ranges and fluxes are given in this paper in the heliocentric frame). As a criterion for smoothness, we adopt the closeness of the residuals to a constant value in terms of rms (root mean square) deviations. Unfortunately, we have had problems in attempting to calibrate the Hα region spectra of NGC 5548 (Peterson et al. 1999 and references therein) by above fashion. We have found that the calibration is too strongly depend on the adopted criterion for smoothness, so these spectra can not be calibrated reliably and unambiguously by using the Hα + [N II] narrow lines. We have concluded that the calibration problems are primarily related to the changes in the shape of the broad emission-line profile under these narrow lines. However, the Hα and [N II] narrow lines in the case of Arp 102B are more prominent with respect to the broad emission Hα profile than that of NGC 5548, so we can expect a less importance of changes in the shape of the broad emission profile. We have compared the scale factors obtained by the direct integration of [O I] and from the Hα + [N II] residuals fitted to a constant and parabola. The scale factors for all the compared pairs of above calibration methods have shown a difference at approximately 98% confidence level with only one point deviated by more than 3σ as was found via the Monte-Carlo simulation. Therefore, we can suspect the presence of systematic errors in the calibration by residuals, although not very large. Thus the calibration based on the Hα + [N II] residuals is much more precise than that of the [O I] direct integration, but should be treated with some caution.

To place the internally calibrated spectra on an absolute flux scale, we have measured the absolute flux of the [O I] λ6300 narrow emission line using the spectra obtained under the low air mass on photometric nights, total of 4 spectra. We have directly integrated a flux within a window of 6434–6474 Å adopting the wavelength zones for a linear pseudocontinuum to be 6417–6434 Å and 6474–6491 Å. The mean [O I] flux was then set to the found absolute value of $(1.76 \pm 0.18) \times 10^{-14}$ ergs cm^{-2} s^{-1}.

The Hα line fluxes were measured by direct integration over the wavelength interval of 6500–6965 Å and above the continuum. Two windows at 6368–6412 Å and 6995–7048 Å were chosen to fit the continuum with a straight line. A mean continuum flux per unit wavelength was determined in these windows, then averaged and designated as F_{6700}.

The observational uncertainties were evaluated as described by Sergeev et al. (1999a). The uncertainties were determined to be, on average, 2.1% and 1.8% for the Hα line and continuum fluxes, respectively. This is not include the possible effect of "seeing", since we have not enough data points to detect

Table 1. Hα line and continuum fluxes

$JD-2440000$	F_{6700}	F(Hα)	Seeing ($''$)
8829.49	178±6	520±12	1.9
8833.43	190 7	528 14	2.6
9070.59	188 7	491 12	1.9
9077.58	196 7	515 12	2.6
9078.57	193 7	500 12	1.9
9189.46	207 7	535 12	1.9
9249.30	177 6	522 13	1.9
9274.22	175 6	519 12	1.9
9275.24	189 6	509 11	1.9
9327.18	203 7	515 14	3.2
9365.65	199 7	527 14	3.3
9454.56	189 7	489 13	1.9
9489.53	197 7	553 15	2.6
9490.46	194 7	530 12	2.1
9537.47	182 6	513 12	1.9
9567.49	206 7	524 14	2.2
9578.48	237 9	548 15	2.8
9623.37	212 8	542 15	1.9
10010.29	186 6	481 12	1.9
10372.29	197 7	495 11	2.2

Note: Units 10^{-17} ergs cm^{-2} s^{-1} Å^{-1} and 10^{-15} ergs cm^{-2} s^{-1}.

this effect and to perform the correction procedure as given by Malkov et al. (1997) and Sergeev et al. (1999a). We have then compared the evaluated errors with those of the point-to-point scattering computed by selecting the pairs of measurements separated by less than 8 days. Despite a low significance of this scattering measured only from the 5 appropriate pairs as well as the relatively large time span adopted, we have decided to put them into exact agreement by adding (in quadrature) to the evaluated uncertainties the values of 1.2% and 3.0% for the Hα line and continuum, respectively. The added uncertainties were primarily attributed to the seeing effects, including tracking errors.

The fluxes with their uncertainties are given in Table 1 and shown in Fig. 1. Although the variations are detectable, since the χ^2 is equal to 43.5 and 69.4 per 19 degree-of-freedom for the Hα and continuum light curves, respectively, their amplitude is extremely low, especially that of Hα line. Taking into account the observational uncertainties, the real rms variations are as small as 2.7% and 5.7% for the Hα line and continuum, respectively.

4. Cross-correlation results

The cross-correlation analysis has been carried out only for the observational period of JD 2449189–JD 2449624, for which the data points are sampled better. Fig. 2 shows the interpolation cross-correlation function (Gaskell & Sparke 1986; White & Peterson 1994) between the Hα and continuum light curves. For any arbitrary time delay, the CCF was calculated by pairing each of the real data points in both time series with linearly interpolated points. The computed CCF has a maximum value of $r_{max} = 0.68$ at the lag of $\tau_{peak} = 6^{+19}_{-96}$ days. The

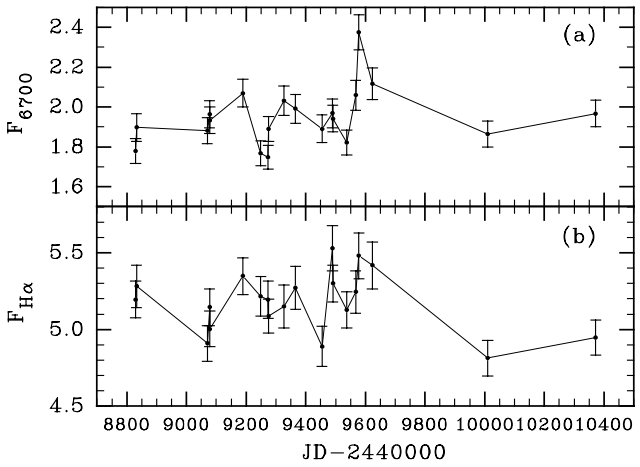

Fig. 1. Light curves are shown for the optical continuum and Hα emission line. Units are 10^{-15} ergs cm^{-2} s^{-1} Å^{-1} and 10^{-13} ergs cm^{-2} s^{-1}.

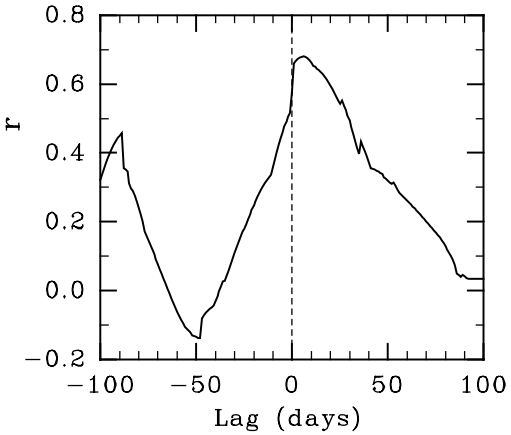

Fig. 2. The interpolation cross-correlation function of the Hα line with the Hα region continuum.

CCF centroid measured above the $0.5\,r_{max}$ level was found to be $\tau_{cent} = 13^{+14}_{-105}$ days. The lag errors were estimated via the Monte-Carlo simulation (Maoz & Netzer 1989). An unusually large negative error is the result of the wrong CCF peak at -89 days (Fig. 2). We have also found that the τ_{peak} greater than 66 days is ruled out at 99% confidence level.

Not surprisingly, the lag value is poorly determined, since the variability amplitude is very low. However, the measured lag is shifted toward positive values, but it is not equal to zero as can be expected for an artificial correlation of our time series via the errors in the scale factors.

5. Narrow emission and absorption lines

Up to this section, no attempt to remove the narrow emission lines superposed on the broad emission profile has been undertaken. Indeed, most of the results given in the next section are independent on any constant contribution to the broad emission profile. However, to determine the relative rms variations we

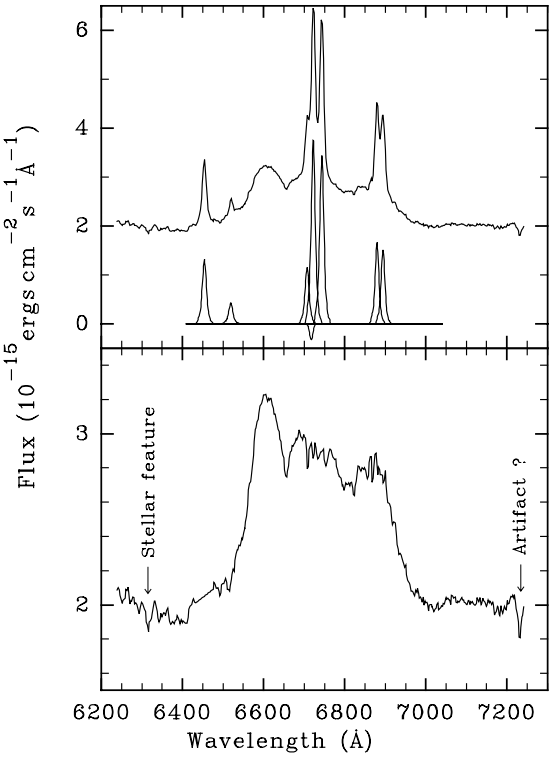

Fig. 3. The narrow emission lines in the mean spectrum of Arp 102B were subtracted by using the [O I] λ6300Å profile as a template to provide the residuals shown in the lower panel to be most smooth. Our fit does not pretend on the exact separation of the broad emission profile, but provides an estimation of the contribution of the [O I], Hα+[N II], and [S II] narrow lines. The fit quality is significantly better when the Hα absorption line is accounted for.

have removed the narrow lines from the Hα broad emission profile as shown in Fig. 3. The narrow lines were fitted by using the [O I] λ6300Å line profile, while the broad line profile segments at the positions of the Hα+[N II] and [S II] narrow lines were fitted to parabolas (not shown). Of course, our fit does not pretend on the exact separation of the narrow lines from the broad emission profiles, since the narrow lines probably differ in their profiles and it might be that the [O I] is not a single, but contaminated with some weak narrow lines. We have found that the fit quality is somewhat worse when the [O III] λ5007Å line profile from a single Hβ region spectrum in our sample is used as a template. The fit quality has been significantly improved (by 54%!) by adding the Hα absorption line. Numerous narrow absorption lines are indeed seen in ultraviolet spectrum of Arp 102B (Halpern et al. 1996). Our mean Arp 102B spectrum clearly shows an absorption feature at λ_{obs} 7231.7Å. This feature was preliminary identified with He I λ7065Å, so its heliocentric redshift is equal to 0.02357, or $V_r = -220\,\mathrm{km\,s^{-1}}$ in the nucleus frame, just the same as found by Halpern et al. (1996) for the ultraviolet absorption lines. However, no this line as well as the lines of the same series (λ4471, λ5875) from which λ5875 should be strongest, are seen in the optical spectrum of Arp 102B present by Halpern et al. (1996). Therefore, we have carefully examined all possible sources of observational errors and found that it might be an artifact due to subtraction of the strong telluric emission line of OH at λ7242Å. A small miscentering or difference in spectral resolution between the spectra of the nucleus and sky background is sufficient to produce P-Cygni or more complex residuals after the sky background spectrum is subtracted off. We have then marked this feature as an "artifact?", although no such residuals are seen near [O I] λ6300Å telluric line that is generally stronger than that of λ7242Å.

From the result of fit we have found the total fluxes of the narrow Hα+[N II] and [S II] emission lines to be 11.3 and 3.98×10^{-14} ergs cm^{-2} s^{-1}, respectively. The [O I] λ6300Å flux was adopted to be 1.76×10^{-14} ergs cm^{-2} s^{-1} (see Sect. 3), while the [O I] λ6364Å flux was set to $\frac{1}{3}$ of the last value. Thus the total contribution of the narrow lines to the measured fluxes of the broad Hα line (the [O I] λ6300Å is outside the integration zone) is of about 1.6×10^{-13} ergs cm^{-2} s^{-1}.

We have found the heliocentric redshifts to be 0.02423, 0.02431, and 0.02439 for the [O I], Hα+[N II], and [S II] narrow emission lines, respectively. The mean value of $z = 0.02431$ has been adopted to transform the heliocentric wavelengths into the nucleus frame velocities.

6. Variability patterns of the Hα broad emission profile

We have subtracted the continuum from each spectrum and analyzed variations at 23 equidistantly spaced bins of the line profile. Fig. 4 shows variability patterns for these bins: the absolute rms variations per unit wavelength, the rms variations normalized to the mean Hα profile (the relative rms variation), and the coefficients of the correlation between the bin fluxes and the continuum flux. The relative rms variations were adjusted for the effects of non-varying narrow lines (Sect. 5). We have also computed the rms variations related to the observational uncertainties: the S/N ratio, the atmospheric dispersion, the errors in the scale factors, and the uncertainties in the continuum subtraction. Methods to estimate these uncertainties are described in the paper of Sergeev et al. (1999a). These errors were then added in quadrature to produce rms deviations expected for the non-variable profile. The observed rms variations are approximately twice as strong as those related to the observational uncertainties (Fig. 4b). The relative rms variations shown in Fig. 4c have been already corrected for the observational uncertainties by subtraction in quadrature. The effect of such a correction is perceptible, but it is not principal at all. We have also computed a correlation matrix containing the correlation coefficients between pairs of the light curves for all bins (Fig. 5).

Although the observed variability amplitude is very low, there are significant changes in the shape of the Hα broad emission-line profile in Arp 102B as can be seen from the Fig. 4 and 5. These changes are very unusual. It is clearly seen from the correlation matrix present in Fig. 5 that the correlation between different pairs of bins is generally poor (light regions), except the same bins or the bins that are closely spaced in wavelength (a dark diagonal line). However, there are two profile segments

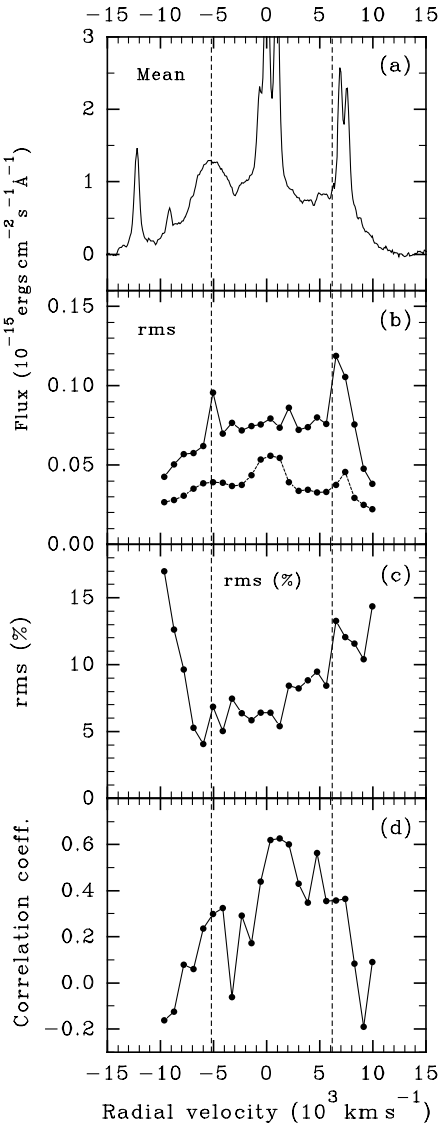

Fig. 4. Variability patterns of the Hα emission-line profile: **a**, **b**, and **c** show, respectively, the mean, absolute rms, and relative rms spectra of Arp 102B. The lower curve in **b** is the rms spectrum related to the observational uncertainties. The correlation coefficients of fluxes at different profile segments with the continuum fluxes are present in **d**. Two dotted lines indicate approximate positions of peaks of the profile bumps. Strong rms variations near the peak of the red bump can be partially attributed to the uncertainties in the removing of the O_2 telluric lines by using spectra of the comparison star.

that show a correlated variability. These segments have a width of no more than 40 Å and located approximately at the peaks of the red and blue bumps of the Hα profile. In particular, when a bin width was set to 10 Å to improve the spectral resolution we have found that the correlation between the bins at observed wavelengths of 6600 Å and 6850 Å is as strong as $r = 0.75$, while the same bin at 6600 Å shows no correlation ($r = 0.01$) with the bin at 6570 Å. Note a lack of correlation for above bins that spaced in wavelength by 30 Å and strong correlation for those spaced by 250 Å! Note also that the flux ratio of bins that closely spaced in wavelength is independent of both the uncertainties in calibration by using narrow lines and the effect of atmospheric dispersion. It is very strange that the well correlated fluxes at the bump peaks have poor correlation with the continuum fluxes (Fig. 4d). The best correlation with the continuum fluxes takes place in the red central part of the Hα profile. The red wing seems to have greater relative amplitude of variability than the blue wing has. The far wings show extremely strong rms variations as large as 10% and even more.

Thus there are at least three kinds of bins that show different behavior: the red central part (relatively strong correlation with the continuum fluxes), the peaks of the red and blue bumps (correlation between their fluxes), and the profile segments that show correlation neither with the continuum fluxes nor with the other profile segments.

Strong variations in the shape of the Hα broad emission-line profile and unusually low variability amplitude of its total flux most likely indicate the matter redistribution in the velocity space. Newman et al. (1997) have considered a hot spot, a region of the disk with excess emissivity. A hot spot model has been first proposed by Zheng et al. (1991) to explain the variations in the broad emission-line profile in 3C 390.3. Indeed, it is easy to reproduce with this model the changes in the relative fluxes of two peaks in Arp 102B. The ratio of their fluxes has shown sinusoidal-like changes for several years (Newman et al. 1997) with a period of about 800 days, and we have verified that our data are in excellent agreement with this result (our result is shown in Fig. 6). To detect the emissivity excess we have subtracted the narrow emission lines (Sect. 5) and continuum and normalized all our profiles to the total Hα flux. We have then subtracted a mean normalized profile from each normalized profile. The residuals rebinned over the time and wavelength are shown as a two-dimensional image in the upper left panel of Fig. 7. Three white horizontal stripes indicate the widest gaps in our time series where the data rebinning by using linear interpolation is too unreliable. We have inspected the individual residuals and found no emission feature at the positions predicted by the hot spot model of Newman et al. (1997). Since the spot angular size was found to be, on average, of about 8°, the emission line profile produced by this spot is relatively narrow and high, especially when the spot has greatest positive or negative radial velocity, while our residuals have only details that are essentially shallower than the expected height of the hot spot line profile. A particular hot spot of Newman et al. (1997) should produce a *narrow* sinusoidal-like track in the velocity–time space, not seen in the upper left panel of Fig. 7. Moreover, the changes in the red-to-blue and other ratios present in Fig. 6 should be periodical, but not sinusoidal, and the center-to-total ratio must have a period shorter by 2 times, because a spot has a zero velocity twice per period. In contrast to this, our results clearly show that all the ratios in Fig. 6 have approximately the same period of about 730 days. However, two light diagonal stripes seen in the upper left panel of Fig. 7 can indicate two emission features propagated through the line profile from its far red wing to the far blue wing, so it can be a signature of rotation. These features can be attributed to the inhomogeneity in the

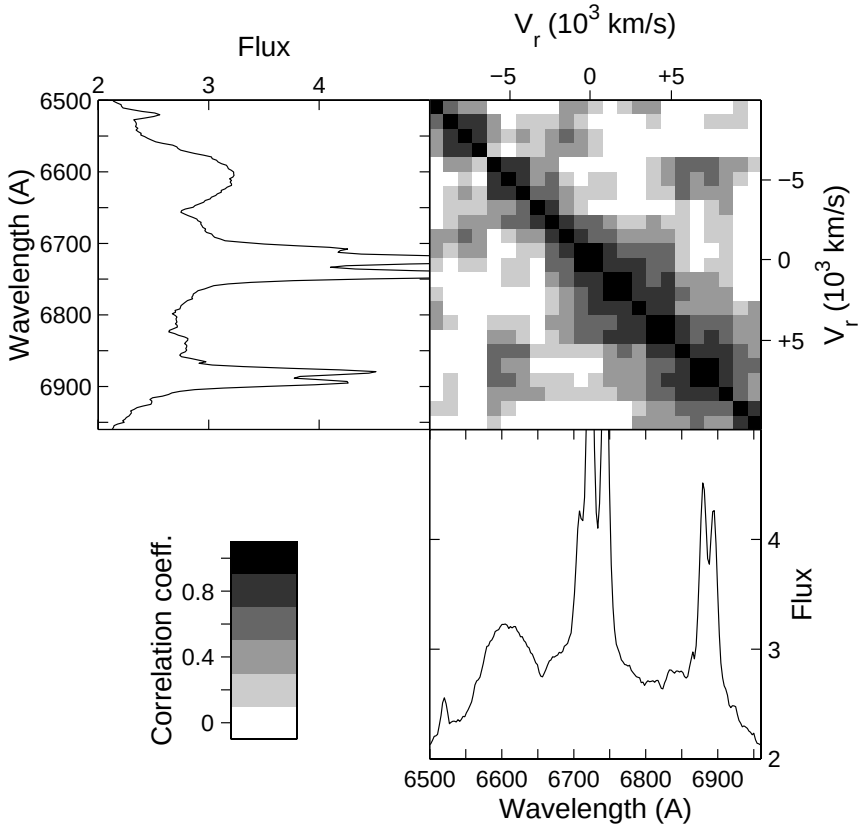

Fig. 5. A correlation matrix, i.e. the correlation coefficients between pairs of the light curves for different Hα profile segments with width of 20 Å are shown as a two-dimensional image in the upper right panel. Also shown are the Arp 102B mean spectrum and the gray color scale for the correlation coefficients.

surface brightness distribution of disk. Another possibility is an ensemble of clouds rotated predominantly at the same plane and produced the same line profile as that of disk. Since a different fraction of the ionized hemisphere of each cloud is seen when the cloud is rotating around the central source, such a phase effect can explain why no tracks seen in the upper left panel of Fig. 7 propagated from blue to red. Adopting a disk inclination angle of $i \approx 30^\circ$ — the case assumed for Arp 102B (e.g. Chen et al. 1989), the line flux of each cloud should vary by two times. We have then test a model in which the observed excess emission are produced by two clouds only. Our computations have shown that the dispersion of the internal cloud velocities should be too large, since a large widths of the observed tracks in Fig. 7. Next we suppose that these tracks are due to a superposition of the randomly distributed clouds that rotated in the same plane. We set the number of clouds per unit surface to be a function of distance r as $n(r) \propto r^{-1}$, the line profile of each cloud was adopted to be a Gaussian, while its flux was set proportional to r^{-2}. For a sake of simplicity we adopted that the profile width produced by each cloud is independent on the azimuth angle, while the flux is undergone a phase effect, assuming clouds are ionized directly by the central source. The possibility that a cloud can sometimes be shaded from the ionizing radiation by other clouds was not taken into account. We have also adopted the inclination angle, the inner radius, and the outer radius to be 32°, $150\,r_g$, and $500\,r_g$, respectively. The excess emission was then modelled by using a Monte Carlo simulation. The typical rotation timescale was found to be similar to that of observed under the central body mass of $3.5 \times 10^8\,\mathrm{M}_\odot$. Fig. 7 shows an excess emission relative to a mean profile as produced by total of 1500 and 5000 clouds emitted the lines with the profile width at half maximum of 2000 km s^{-1} and 400 km s^{-1}, respectively. The relative rms variations shown in the bottom panels of Fig. 7 are in good agreement with the observed variations, although the last should include the line response to the ionizing continuum changes. So, the observed changes in the Hα line profile can be dominated by the redistribution of the rotating matter.

We have also examined whether our model is able to reproduce observed sinusoidal changes shown in the left panels of Fig. 6. Three independent Monte-Carlo realization in terms of the model with 1500 clouds were computed to simulate observations for a time span of 20000 days. We have found several appropriate episodes in each realization that show sinusoidal-like changes with some difference in phase in all ratios shown in Fig. 6 except the center-to-total ratio. The last ratio shows generally faster variations. We were only able to explain sinusoidal-like changes with the same period for all considered ratios when the inclination angle is set to 90° (edge-on configuration), while the mass, internal radius, and external radius are set to $5.22 \times 10^7\mathrm{M}_\odot$, $534\,r_g$, and $1780\,r_g$, respectively, to keep the same period of rotation and approximately the same profile width (the profile shape can not be kept exactly the same because of difference in the relativistic and gravitational effects). The simulation results are shown in the three right columns of panels of Fig. 6. In this configuration, any cloud's emission feature is only seen at the profile center when propagating from

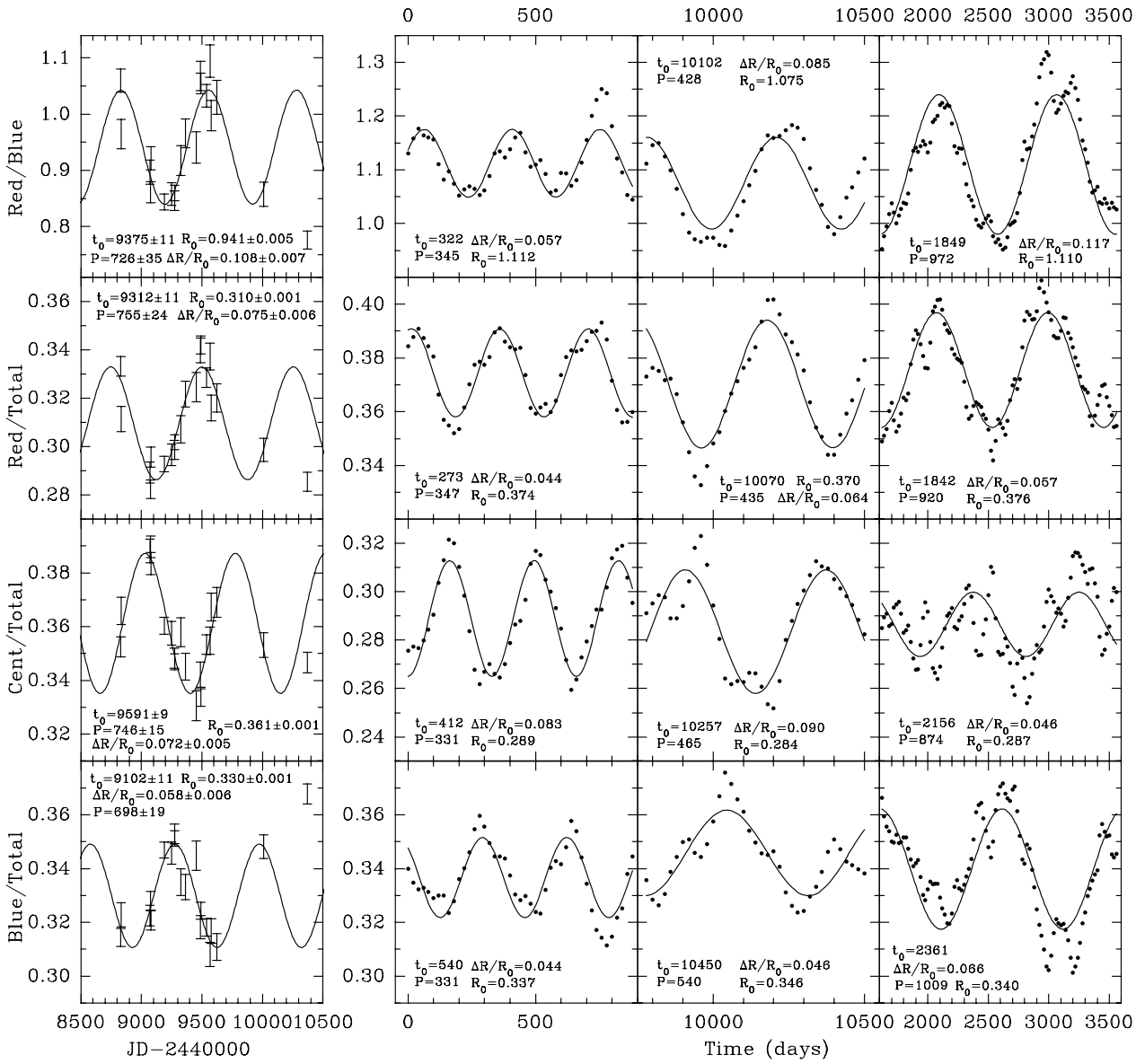

Fig. 6. Ratios of fluxes at four segments of the Hα line profile designated as Blue ($\lambda\lambda_{obs}$6550–6660), Cent ($\lambda\lambda_{obs}$6660–6790), Red ($\lambda\lambda_{obs}$6790–6940), and Total ($\lambda\lambda_{obs}$6550–6940) are shown. The first column of panels present observational results. The solid line is a fit to a sinusoidal function: $R = \Delta R sin[2\pi(t-t_0)/P] + R_0$. The fit parameters are shown in each panel. The last data point is excluded. The next three columns present results based on our cloud model (see text) and obtained by three independent Monte-Carlo realizations that simulate observations for a period of 20000 days starting with 0. Only a single fragment from each realization was selected to show that sinusoidal-like changes are possible in this model.

the red side to the blue side, i.e. once per period, because in the opposite position the ionized cloud's hemisphere is fully hidden from observer. The edge-on configuration is more suitable in all respects to reproduce changes in the profile shape, but it gives a profile shape less asymmetric than the observed profile.

7. Summary and discussion

The broad Hα line profile in Arp 102B shows unusual changes in its shape. Strong variations at different bins of the Hα profile, while its total flux is changed only a little can be explained by the rotational redistribution of matter emitted the broad lines. Some indications of the rotation are indeed seen from the upper left panel of Fig. 7 where the evolution of the excess emission is shown. Also, different sections of the line profile generally show very poor correlation between themselves as well as with the continuum flux, while the correlation between the line integrated flux and continuum flux is much better. Our results, however, are strongly inconsistent with a model of a *single* hot spot claimed by Newman et al. (1997), but can be explained by a model in which there are thousands of clouds rotating predominantly in the same plane. In terms of this model, we are

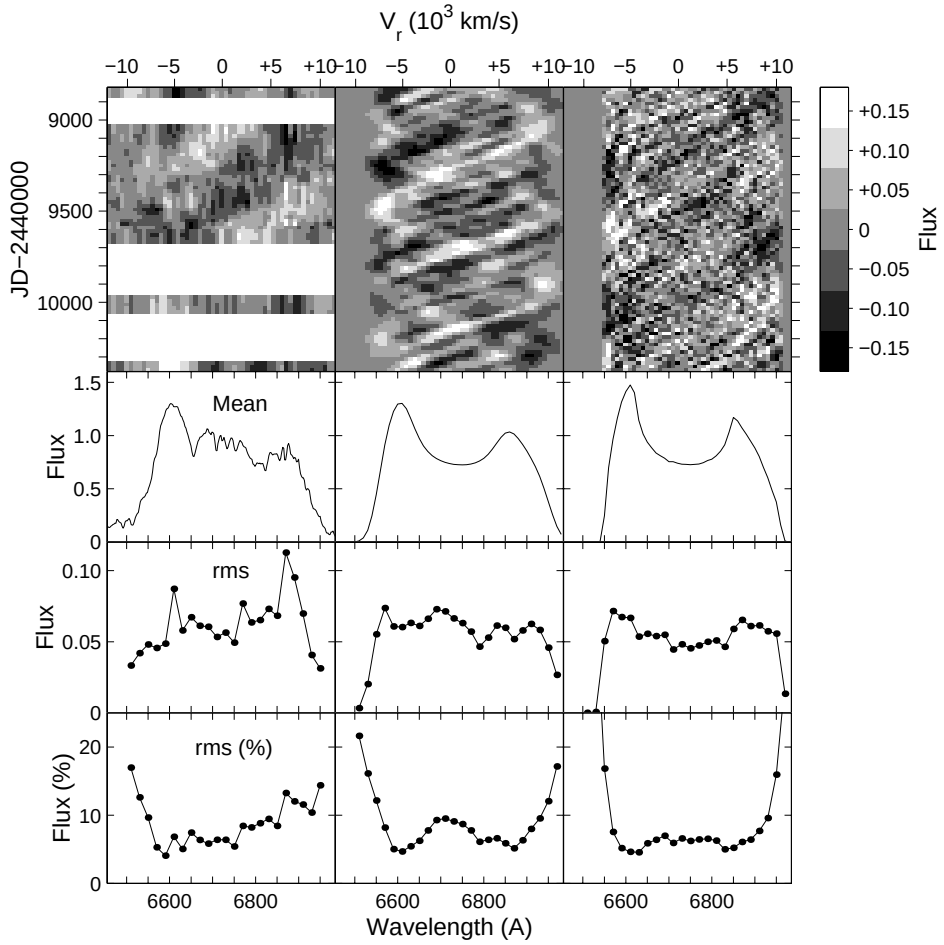

Fig. 7. The evolution of the excess emission of the Hα line profile is shown in the first row of panels as two-dimensional images (see text). Also shown are the mean, absolute rms, and relative rms spectra. The first column of panels present results based on observations. The second and third columns present results of a model in which there are total of 1500 and 5000 rotating clouds, respectively (see text).

able to reproduce qualitatively the observed variations of the profile shape and the sinusoidal changes in the relative height of bumps, but the changes in the center-to-total ratio can only be explained under assumption that the inclination angle to the line-of-sight is somewhat less than usually believed. Note, that our simulation results can explain not only the same period for all considered ratios, but the phase differences in their sinusoidal variations are in excellent agreement (not exceed ± 0.1 of period!) with observations too. Although the probability to find sinusoidal changes for all considered ratios is small (cf. time intervals in Fig. 6 and the total simulated time span of 20000 days), it can not be treated as negligible. Also, the simulated relative rms changes in the Hα line profile are *quantitatively* very similar to the observed rms changes.

The required internal velocity dispersion in individual clouds of $\sim 10^3$ km s^{-1} is a most difficult point in our model. We do not know what physical processes responsible for it and how to prevent clouds from a dissipation in a short time. Can these clouds be identified with the bloated stars of Alexander (1997)? In this scenario, the number of bloated stars is believed to be somewhat greater (< 50000) than the number of our clouds, while the wind velocity to be much less than 10^3 km s^{-1}. Emission lines produced by clouds can also be broadened by electron scattering in the intercloud media as often believed in accretion disk models of BLR.

To provide an appropriate covering factor, the clouds should rotate not exactly in the same plane, but only "predominantly". We have evaluated that a cloud in our ensemble of 1500 clouds should have a size greater than 0.2 light days to provide covering factor of 0.1 believed to be sufficient to produce emission lines observed in spectra of AGNs. We have then estimated that a mean cloud should collide, on average, for a time span of 13 years, if the cloud system is flat, or for a time span of 24 years, if the inclination of the cloud orbits has rms of 20°. Although it is not clear what impact parameter and collision velocity are necessary to destroy a cloud completely, the cloud life time seems to be small, and the cloud formation rate must be high. This problem is relevant not only for our particular model, but for any model of rotating clouds with large covering factor. The rate of cloud collisions increase toward internal radius, where continuous disk may be formed.

In principle, the same simulation results can be obtained from accretion disk models, where "clouds" are inhomogeneities in the disk surface brightness (hot spots). The only difference is that the hot spot brightness has no phase effect, so moving excess emissions should propagate from the blue side to the red side as well as vice versa. Also, with a disk model, it

is more difficult to explain the sinusoidal changes in the center-to-total ratio with the same period as that of other considered ratios.

We should also note, that two narrow profile segments centered approximately at the peaks of bumps show a correlated variability (Fig. 5), but it is not clear whether this correlation is accidental or it has a physical meaning.

There is an inconsistency in the rms variations of 2.7% and 5.7% for the line and continuum, respectively. The last value should be enlarged by taking into account the host galaxy contribution. We have measured the strength of the Ca I λ6162Å stellar feature and estimated the stellar contribution through our entrance aperture to be at least half of the observed flux. Thus most of the line emission does not follow the continuum changes, and this emission can be attributed either to the collisional excitation or to fully ionized clouds. The fully ionized clouds, however, do not show a phase effect considered in the previous section to explain the observed evolution of the excess emission. The BLR in Arp 102B may actually consist of an accretion disk with inhomogeneity in its surface brightness and an "usual" BLR, which follows the continuum changes. The line component that respond to the continuum changes is probably more prominent in the red central part of the line profile, where the correlation with the continuum fluxes is somewhat better (Fig. 4). The central component is indeed seen in Fig. 3, but it is difficult to retrieve the shape and width of its profile, because of variations related to the matter redistribution dominate those driven by continuum changes. The widely used rms profile is not applicable in this case. More appropriate seems to be a profile of the variable component that follows the line total flux or respond to the continuum variations as defined by Sergeev et al. (1994). Its profile width was found to be somewhat narrower than the width of the entire profile (Sergeev et al. 1999b).

The results of our monitoring campaign reveal evidences for a disk model of BLR in Arp 102B. We have considered two possibilities: a continuous disk with inhomogeneities in its surface brightness and a system of clouds rotating predominantly in the same plane. How widely a disk model can be applied to other targets with a double-peaked profiles? We believe that this model is insufficient to explain the observed variety of bumps, even if they are closely similar to that of Arp 102B. According to our preliminary results, 3C 390.3 shows quite different patterns of the evolution of profile shapes of the broad Balmer lines as compared with Arp 102B, although their profile shapes are very similar. A two-dimensional image computed for the Hα line in 3C 390.3 by the same way as in the upper left panel of Fig. 7, shows strong changes in the profile shape, including changes in the relative height of bumps, but it does not show moving emission features except, probably, one broad feature in the far red wing that moves slowly toward positive velocities. The case of Pictor A also present a problem (Sulentic et al. 1995) in attempting to attribute the double-peaked profiles to the accretion disk. First, the red bump in Pictor A is stronger that the blue bump, not consistent with a circular disk. And second, the residuals of several individual Hα line profiles show very broad features and strong difference in the variations of the red and blue bumps at different epochs. Such very broad features are difficult to reconcile with a hot spot (it should occupy of about 1/4 of the disk surface), and even with a model of many hot spots or clouds rotating predominantly in the same plane.

We believe that the future monitoring programs will shed a light to a different behavior of the double-peaked profiles in different objects as well as to their origin.

Acknowledgements. We are thankful to our referee, Dr. J. Halpern, for valuable remarks.

References

Alexander T., 1997, MNRAS 285, 891
Blandford R.D., McKee C.F., 1982, ApJ 255, 419
Chen K., Halpern J.P., 1989, ApJ 344, 115
Chen K., Halpern J.P., Filippenko A.V., 1989, ApJ 339, 742
Collin-Souffrin S., Dumont A.M., 1990, A&A 229, 292
Emmering R.T., Blandford R.D., Shlosman I., 1992, ApJ 385, 460
Eracleous M., Halpern J.P., 1994, ApJS 90, 1
Eracleous M., Livio M., Halpern J.P., Storchi-Bergmann T., 1995, ApJ 438, 610
Eracleous M., Halpern J.P., Gilbert A.M., et al., 1997, ApJ 490, 216
Gaskell C.M., 1988, In: Miller H.R., Witta P.J. (eds.), Proc. Georgia State University Conf. on Active Galactic Nuclei, Springer-Verlag, New York, p. 61
Gaskell C.M., Sparke L.S., 1986, ApJ 305, 175
Goad M., Wanders I., 1996, ApJ 469, 113
Halpern J.P., Eracleous M., Filippenko A.V., et al., 1996, ApJ 464, 704
Kaspi S., Maoz D., Netzer H., et al., 1996, ApJ 470, 336
Malkov Yu.F., Pronik V.I., Sergeev S.G., 1997, A&A 324, 904
Maoz D., Netzer H., 1989, MNRAS 236, 21
Maoz D., Netzer H., Mazeh T., et al., 1991, ApJ 367, 443
Newman J.A., Eracleous M., Filippenko A.V., Halpern, J.P., 1997, ApJ 485, 570
Oke J.B., 1987, In: Zensus J.A., Pearson T.J. (eds.), Superluminal radio sources. Cambridge University Press, Cambridge, p. 267
Perez E., Penston M.V., Tadhunter C., Mediavilla E., Moles M., 1988, MNRAS 230, 353
Peterson B.M., 1994, In: Gondhalekar P.M., Horne K., Peterson B.M. (eds.), Reverberation Mapping of the Broad-Line Region in Active Galactic Nuclei. ASP Conference Series 69, 1
Peterson B.M., Barth A.J., Berlind P., et al., 1999, ApJ 510, 659
Sergeev S.G., 1992, Ap&SS 197, 77
Sergeev S.G., Malkov Yu.F., Chuvaev K.K., et al., 1994, In: Gondhalekar P.M., Horne K., Peterson B.M. (eds.), Reverberation Mapping of the Broad-Line Region in Active Galactic Nuclei, ASP Conference Series 69, 199
Sergeev S.G., Pronik V.I., Sergeeva E.A., Malkov Yu.F., 1999a, ApJS 121, 159
Sergeev S.G., Pronik V.I., Sergeeva E.A., et al., 1999b, AJ 118, 2658
Sulentic J.W., Marziani P., Zwitter T., et al., 1995, ApJ 438, L1
van Groningen E., Wanders I., 1992, PASP 104, 700
Wanders I., Peterson B.M., 1996, ApJ 466, 174
White R.J., Peterson, B.M., 1994, PASP 106, 879
Zheng W., Veilleux S., Grandi S.A., 1991, ApJ 381, 418